

1 **Data-based estimates of ocean carbon uptake biased high from neglect of submonthly**  
2 **atmospheric pressure variability**

3 Authors: Jeanne Dombret<sup>1</sup>, Hugo Bellenger<sup>1\*</sup>, Xavier Perrot<sup>1</sup>, Laëtitia Parc<sup>1</sup>, Lester  
4 Kwiatkowski<sup>2</sup>, Frédéric Chevallier<sup>3</sup>, Laurent Bopp<sup>1</sup>, Marion Gehlen<sup>3</sup>, Roland  
5 Séférian<sup>4</sup>, Sarah Berthet<sup>4</sup> and James C. Orr<sup>3</sup>

6 Affiliations :

7 <sup>1</sup> Laboratoire de Météorologie Dynamique, LMD-IPSL, École Normale Supérieure,  
8 Université PSL, École polytechnique, Institut Polytechnique de Paris, Sorbonne  
9 Université, CNRS, Paris France.

10 <sup>2</sup> Laboratoire d'Océanographie et du Climat : Expérimentations et Approches Numériques,  
11 LOCEAN-IPSL, Sorbonne Université-CNRS-IRD-MNHN, Paris, France

12 <sup>3</sup> Laboratoire des Sciences du Climat et de l'Environnement, LSCE-IPSL, CEA-CNRS-UVSQ,  
13 Université Paris Saclay, Gif-sur-Yvette, France

14 <sup>4</sup> Centre National de Recherches Météorologiques (CNRM), Université de Toulouse, Météo-  
15 France, CNRS, Toulouse, France.

16 Correspondance : Hugo Bellenger (hugo.bellenger@lmd.ipsl.fr)

17

18 Manuscript submitted to Biogeosciences

19 **Key points**

- 20 • Neglect of submonthly variability of atmospheric pressure in data-based ocean carbon  
21 sink estimates causes a positive bias of 0.12 Pg C yr<sup>-1</sup>
- 22 • This bias represents on average 25% of the gap between model and data-based estimates  
23 of the sink between 2008 and 2019

- 24 • This bias is driven by the covariance between wind speed and atmospheric pressure,  
25 85% of which stems from the southern midlatitudes

## 26 **Abstract**

27 Current estimates of the global ocean carbon sink based on measurements of CO<sub>2</sub> fugacity are  
28 inconsistent with those obtained from global ocean biogeochemistry models. Here we  
29 investigate how this gap might change by more fully accounting for submonthly variability in  
30 observation-based estimates, a step closer to the roughly hourly frequencies used in models.  
31 While these data-based estimates use hourly to 6-hourly wind speeds to compute the air-sea  
32 CO<sub>2</sub> flux, other input variables are available only at monthly resolution. Thus, they neglect  
33 high-frequency variability in key variables such as atmospheric pressure associated with  
34 synoptic events such as storms. To evaluate this error, we compare flux estimates from  
35 observational data sets with different temporal resolutions. Accounting for hourly variations in  
36 atmospheric pressure and daily variations in sea surface temperature, a data-based approach  
37 reduces the estimated global carbon uptake by 0.12 Pg C yr<sup>-1</sup>, closing 25% of the average gap  
38 between observation-based and model estimates. This reduction results from proper accounting  
39 of the covariance between wind speed and atmospheric pressure, particularly in the southern  
40 extratropics.

## 41 **Plain language summary**

42 Estimates of ocean CO<sub>2</sub> uptake based on atmospheric and oceanic observations typically rely  
43 on monthly averages, except for wind speed. This means they miss the effects of shorter-term  
44 events such as storms, unlike models. Here we account for the impact of this short-term  
45 variability on ocean carbon uptake and find that estimated uptake is reduced, mainly because  
46 storms lower atmospheric pressure. This refinement closes about 25% of the gap between  
47 observation-based and model-based estimates.

## 48 1. Introduction

49 The ocean absorbs one-fourth of anthropogenic CO<sub>2</sub> emissions, playing a major role in the  
50 global carbon cycle. It is estimated to have absorbed 2.9 Pg C yr<sup>-1</sup> of anthropogenic carbon  
51 during 2014-2023 based on the Global Carbon Budget (GCB, Friedlingstein et al. 2025). But  
52 this average value comes with a spread of more than 1 Pg C yr<sup>-1</sup> between the lowest and highest  
53 estimates. The GCB is updated annually to reflect the evolution in the data and methods used  
54 to obtain the latest estimates of global carbon emissions and carbon storage in different  
55 reservoirs (sinks). Its ocean estimate relies on two different approaches.

56 The first approach uses global ocean biogeochemistry models (GOBMs), each of which  
57 couples a global-scale, general ocean circulation model to an ocean carbon cycle component.  
58 GOBMs simulate ocean transport of dissolved inorganic carbon (DIC) and total alkalinity  
59 (Alk), from which is calculated surface ocean CO<sub>2</sub> fugacity ( $f\text{CO}_{2\text{ sea}}$ ), a variable nearly identical  
60 to the ocean partial pressure of CO<sub>2</sub> ( $p\text{CO}_{2\text{ sea}}$ ). From that, the models compute the difference  
61 relative to the atmospheric CO<sub>2</sub> fugacity ( $f\text{CO}_{2\text{ atm}}$ ), multiplying that difference by a gas transfer  
62 velocity times the solubility to compute the air-sea CO<sub>2</sub> flux. The simulated air-sea CO<sub>2</sub> flux  
63 is affected by multiple physical atmospheric variables since the gas transfer velocity is often  
64 parameterized as a quadratic function of wind speed and  $f\text{CO}_{2\text{ atm}}$  depends in part on atmospheric  
65 pressure and vapor pressure. GOBMs are typically forced by atmospheric reanalyses having  
66 hourly to 6-hourly timesteps. Nonetheless, simulated ocean uptake of anthropogenic carbon in  
67 GOBMs is only weakly sensitive to uncertainties in the gas transfer velocity. For example, a  
68 doubling of the gas transfer velocity led to only a 9% increase in simulated ocean uptake of  
69 anthropogenic carbon (Sarmiento et al., 1992). The extra CO<sub>2</sub> added to the ocean from enhanced  
70 gas exchange is not transported away from the surface quickly enough, thus increasing the  
71 simulated  $f\text{CO}_{2\text{ sea}}$  and reducing the change in the air-sea flux, a key feedback inherent not only

72 in models but also in the real ocean. While models have their own problems, such as biases in  
73 simulated circulation fields, they are insensitive to the magnitude of the gas transfer velocity.

74 The second approach uses observation-based products for  $fCO_{2sea}$  rather than modeled  
75 fields. These data products rely on millions of in situ measurements of  $fCO_{2sea}$  archived in the  
76 Surface Ocean CO<sub>2</sub> Atlas (SOCAT, Bakker et al., 2016). Many groups have used this unevenly  
77 spaced data to produce evenly spaced gridded data products, mapping it typically to a  $1^\circ \times 1^\circ$   
78 grid with monthly resolution and filling missing grid cells based on a series of global predictors,  
79 e.g., sea surface temperature and mixed-layer depth, obtained from satellite products and  
80 atmospheric and oceanic reanalyses (Landschützer et al., 2016; Rödenbeck et al., 2022; Chau  
81 et al., 2024; Watson et al., 2020; Zeng et al., 2022; Iida et al., 2021; Gregor et al., 2024; Gloege  
82 et al., 2022; Gregor et al. 2019). Using observed rather than simulated  $fCO_{2sea}$  is an advantage  
83 since it reflects the real ocean's air-sea interaction. But it comes with a disadvantage: the data-  
84 based approach cannot benefit from the previously mentioned feedback between the flux and  
85  $fCO_{2sea}$ . Thus, compared to the GOBMs, data-based estimates of air-sea CO<sub>2</sub> fluxes are more  
86 sensitive to errors in the bulk flux parameterization, with associated uncertainties scaling  
87 proportionally to the imposed gas transfer velocity (Gloege et al. 2025, Jersild and Landschützer  
88 2024).

89 It is estimated that the ensemble mean 1- $\sigma$  uncertainty for the 10 models is 0.5 Pg C yr<sup>-1</sup>  
90 while that for the 8 data products is 0.6-0.7 Pg C yr<sup>-1</sup> considering both random and systematic  
91 uncertainties (Friedlingstein et al., 2025; Ford et al., 2024). Moreover, there is a systematic  
92 discrepancy between the two approaches, where the average sink from data-based products is  
93 0.5 Pg C yr<sup>-1</sup> larger than that from GOBMs. Friedlingstein et al. (2025) suggest a possible 10%-  
94 20% underestimate from the GOBMs for the ocean uptake of anthropogenic carbon owing to  
95 several potential problems: an overestimated Revelle factor, salinity biases in the Southern  
96 Ocean, an underestimated penetration of carbon into the ocean interior from weak vertical

97 mixing and transport, and a delayed beginning for the anthropogenic perturbation, after the  
98 actual start of the industrial era (see Bronselear et al., 2017, Terhaar et al. 2022, Terhaar et al.  
99 2025).

100 Other potential sources of model-data discrepancy come from the data-based approach.  
101 First, there is the  $0.65 \pm 0.15 \text{ Pg C yr}^{-1}$  that must be added to the data-based estimates to back  
102 calculate the anthropogenic carbon flux from the total flux by removing the global effect of the  
103 net preindustrial outgassing driven by the natural imbalance between riverine input and  
104 sediment loss of carbon (Aumont et al., 2001; Regnier et al., 2022), as discussed by DeVries et  
105 al. (2023), Perez et al. (2024) and Planchat et al. (2025). Another important source of  
106 uncertainty is the sparsity of SOCAT measurements in some key regions such as the Southern  
107 Ocean (Hauck et al., 2020, 2023; Ford et al., 2024). Finally, discrepancies may also stem from  
108 the very different temporal resolutions of the two approaches. While GOBMs compute air-sea  
109  $\text{CO}_2$  fluxes with a time step on the order of an hour, the data-based products used in GCB 2024  
110 generally rely on monthly averaged variables. Fortunately, the data-based products do account  
111 for the effect of submonthly wind-speed variance by using monthly means of the square of  
112 observed 1- to 6-hourly wind speed when computing the gas transfer velocity. But they neglect  
113 nonlinearities stemming from submonthly variability of other physical drivers, including  
114 atmospheric pressure, sea surface temperature, and sea surface salinity.

115 To address this limitation, Gregor et al. (2024) developed a higher-frequency data  
116 product computing the  $\text{CO}_2$  flux with 8-day temporal resolution, but they also showed its use  
117 had minimal effect on the resulting global sink estimate. Unfortunately, an 8-day frequency still  
118 does not resolve intense meteorological events, such as tropical cyclones and extratropical  
119 storms, which drive variations in atmospheric and oceanic variables on shorter time scales.  
120 Previous case studies have shown that tropical cyclones can cause substantial regional ocean  
121 carbon uptake (Gregor et al., 2024) or outgassing (Bates et al., 1998; Huang & Imberger, 2010),

122 depending largely on the initial sign of the CO<sub>2</sub> fugacity difference at the air-sea interface. Yet  
123 the resulting global contribution of tropical cyclones to the ocean carbon sink is negligible  
124 (Lévy et al. 2012) because they mostly occur in regions with weak air-sea differences in  $fCO_2$   
125 and because they increase CO<sub>2</sub> fluxes both into and out of the ocean, nearly canceling one  
126 another. Extratropical studies with data from floats and gliders indicate that storms in the  
127 Southern Ocean can provoke outgassing anomalies over 1-3 days, driven by concomitant  
128 variations in wind speed, atmospheric pressure, and DIC concentrations (Carranza et al., 2024;  
129 Nicholson et al., 2022). The Argo float-based estimates suggest that Southern Ocean storms  
130 may reduce the global carbon sink by up to 0.057 Pg C yr<sup>-1</sup> (Carranza et al., 2024). But storms  
131 represent only a part of the submonthly phenomena. It remains uncertain how high-frequency  
132 variability, if it were properly accounted for in data-based approaches, would affect resulting  
133 estimates of the air-sea CO<sub>2</sub> flux at the global scale.

134         Although submonthly and particularly synoptic variability of ocean biogeochemical  
135 variables ( $fCO_2$ , DIC...) cannot yet be constrained at the global scale due to the scarcity of  
136 observations, such is not the case for physical variables including not only wind speed but also  
137 atmospheric pressure, sea surface temperature and salinity. Here we ask how much this  
138 submonthly variability might affect observation-based estimates of the global ocean carbon  
139 sink, particularly in mid-latitudes where storms induce outgassing through simultaneous  
140 decreases in atmospheric pressure and increases in wind speed. Our aim is to quantify the  
141 importance of this effect, identifying the responsible non-linearities between variables and the  
142 regions where they dominate.

143

## 144         **2. Methods**

145

### 146         **2.1 CO<sub>2</sub> flux calculations**

147 Consistent with the GCB, our data-based air-sea CO<sub>2</sub> flux  $F$  is computed as

$$148 \quad F = k_{660}(u)A(T, S)(fCO_{2atm} - fCO_{2sea}). \quad (1)$$

149 where  $k_{660}$  is the gas transfer (piston) velocity at 20°C,  $fCO_{2atm}$  and  $fCO_{2sea}$  are the  
150 fugacities of CO<sub>2</sub> in the atmosphere and the ocean, and  $A = K_0(T, S) \left(\frac{Sc(T)}{660}\right)^{-1/2}$  with  $K_0$  being  
151 the solubility of CO<sub>2</sub> in seawater computed from the sea surface temperature ( $T$ ) and salinity  
152 ( $S$ ) (Weiss, 1974), and the Schmidt number ( $Sc$ ) ratio is used to adjust the wind-speed  
153 formulation for gases other than CO<sub>2</sub> and for temperatures other than 20°C (Wanninkhof, 2014).  
154 Positive fluxes indicate an air-to-sea CO<sub>2</sub> flux. The  $k_{660}$  is calculated using a quadratic function  
155 of the 10-m wind speed  $k_{660} = au^2$  (Wanninkhof, 1992), and  $u$  is the wind speed at 10 m. As  
156 for  $a$ , it is an empirical scaling constant adjusted for each wind dataset so that the corresponding  
157 global value of  $k$  (i.e.,  $k_{660}$  normalized to different temperatures with the Schmidt number ratio  
158 above) averages 16.5 cm hr<sup>-1</sup> over the ice-free ocean as derived from the observed global bomb  
159 <sup>14</sup>C inventory (Naegler, 2009). Since it is based on the real ocean inventory of bomb <sup>14</sup>C, this  
160 scaling approach should inherently account for the effects of submonthly variability of all  
161 variables that affect the gas transfer velocity; however there is a 20% uncertainty associated  
162 with the bomb <sup>14</sup>C inventory and thus  $k$ .

163 The CO<sub>2</sub> fugacity in the atmosphere,  $fCO_{2atm}$ , is the partial pressure of CO<sub>2</sub> corrected for the  
164 non-ideal behaviour of the gas. The  $fCO_{2atm}$ , (in  $\mu$ atm) is computed from the mixing ratio (or  
165 mole fraction) of CO<sub>2</sub> (in ppm), which is measured in dried air, as follows

$$166 \quad fCO_{2atm} = \phi_{CO_2}(P_{atm}, T)X_{CO_2} \left(P_{atm} - P_{vap}(T, S)\right) \quad (2)$$

167 where  $\phi_{CO_2}$  is the fugacity coefficient from Weiss (1974),  $X_{CO_2}$  is the CO<sub>2</sub> mole fraction in dry  
168 air (ppm),  $P_{atm}$  is the surface atmospheric pressure (atm), and  $P_{vap}$  is the partial pressure of

169 water vapor (atm) from Weiss & Price (1980), an empirical function of  $T$  and  $S$  assuming that  
170 the air is fully saturated (100% humidity) just above the air-sea interface.

171 For simplicity, in contrast with GCB data-based product, our oceanic fugacity  $fCO_{2sea}$   
172 is not from an ocean  $fCO_2$  observation product but is instead computed from gridded products  
173 of  $T$ ,  $S$ , DIC, Alk, and total inorganic phosphorus and silicon concentrations ( $[P]$  and  $[Si]$ ) using  
174 mocsy (Orr & Epitalon, 2015). This simplification enables us to evaluate the impact of  
175 submonthly variability of  $T$  and  $S$  on  $fCO_{2sea}$  while maintaining the basic GCB data-based  
176 approach.

177 We use hourly fields of wind speed  $u$  and surface pressure  $P_{atm}$ , and daily fields of sea  
178 surface temperature  $T$  and sea ice concentration from the fifth generation ECMWF reanalysis  
179 (ERA5, Hersbach et al., 2020) at  $0.25^\circ \times 0.25^\circ$  spatial resolution. In the gas transfer velocity  
180 formulation, the empirical scaling constant  $a$  is taken to be 0.271 as computed for the ERA5  
181 wind speed field by Fay et al. (2021). We also use the bulk daily sea surface temperature rather  
182 than the hourly sea-surface skin temperature to be consistent with current GCB data-based  
183 estimates. All but one of those estimates use bulk sea surface temperature. Thus, we do not  
184 include effects of diurnal warming and cool skin that have been addressed in previous studies  
185 (Watson et al. 2020, Dong et al. 2022, Bellenger et al. 2023). Sea-surface salinity  $S$  is taken  
186 from the Multi Observation Global Ocean Sea Surface Salinity and Sea Surface Density dataset  
187 (Droghei et al., 2018) with  $0.25^\circ \times 0.25^\circ$  spatial resolution and 8-day temporal resolution.  
188 Atmospheric  $CO_2$  dry air mole fraction  $X_{CO_2}$  is from the NOAA Greenhouse Gas Marine  
189 Boundary Layer Reference (Lan et al., 2023), provided as  $4.5^\circ$  latitudinal bands at a temporal  
190 resolution of  $\sim 8$  days. For  $X_{CO_2}$ , we computed its monthly means because of the limited  
191 observational network used to produce this global data set, thus leaving the impact of its  
192 submonthly variability for future studies. Fields of DIC and Alk are from OceanSODA-ETHZ  
193 (Gregor & Gruber, 2021), which has  $1^\circ \times 1^\circ$  spatial resolution and monthly temporal resolution.

194 Fields of  $[P]$  and  $[Si]$  are from a monthly climatology (Broullón et al., 2019) derived from the  
 195 2013 World Ocean Atlas dataset (Boyer et al., 2013), also on a  $1^\circ \times 1^\circ$  grid. Before computing  
 196 fluxes, all datasets are regridded to a common  $0.25^\circ \times 0.25^\circ$  grid using bilinear interpolation.  
 197 Air-sea  $\text{CO}_2$  fluxes are calculated from 2009 to 2018 and, for simplicity, only for latitudes  
 198 between  $60^\circ\text{S}$  and  $60^\circ\text{N}$ , thus avoiding most sea-ice covered areas. Calculations consider only  
 199 the time steps when grid cells have no ice cover. Regions poleward of  $60^\circ$  contribute only  
 200 marginally to the global sink (Takahashi et al., 2009). Table 1 summarizes the data used in this  
 201 study.

202 To study the sensitivity of the global ocean carbon sink to the submonthly variability  
 203 that is neglected in GCB data-based products, we computed two estimates: (1) our reference,  
 204 using monthly averages for all variables except for wind speed, which as in GCB already  
 205 accounts for submonthly wind speed variance; and (2) our test case, using instead higher  
 206 temporal resolution data for atmospheric pressure, sea-surface temperature, and sea surface  
 207 salinity. Consistent with the temporal resolution of GCB 2024 data products, the reference flux  
 208  $F_{ref}$  is calculated using the monthly mean of the squared wind speed computed from hourly  
 209 data  $\overline{u^2}$  and monthly means of the other variables:

$$210 \quad F_{ref} = a\overline{u^2}A(\overline{T}, \overline{S}) \Delta f\text{CO}_2 \left( \overline{P_{atm}}, \overline{T}, \overline{S}, \overline{X_{\text{CO}_2}}, \overline{DIC}, \overline{Alk}, \overline{[P]}^c, \overline{[Si]}^c \right) \quad (3)$$

211 The overbar denotes a monthly mean, while the appended  $c$  superscript indicates a  
 212 climatological monthly mean. The high-frequency flux  $F_h$  is calculated hourly using each  
 213 variable at its highest available temporal resolution (hourly  $u$  and  $P_{atm}$ , daily  $T$ , 8-daily  $S$ , and  
 214 monthly for all others). We compare  $F_{ref}$  to  $\overline{F_h}$ , the monthly mean of  $F_h$  :

$$215 \quad \overline{F_h} = \overline{a u^2 A(T, S) \Delta f\text{CO}_2 \left( P_{atm}, T, S, X_{\text{CO}_2}, DIC, Alk, [P]^c, [Si]^c \right)} \quad (4)$$

216 To further assess the causes of differences, we also compare  $F_{ref}$  and  $\overline{F_h}$  to the monthly  
 217 averages of two intermediate air-sea CO<sub>2</sub> fluxes: (1)  $\overline{F_p}$  which is computed like  $\overline{F_h}$  but using  
 218 hourly  $P$  and monthly  $T$  and  $S$  and (2)  $\overline{F_{p,T}}$ , which is computed using hourly  $P_{atm}$ , daily  $T$ , and  
 219 monthly  $S$ . Then the difference  $\overline{F_p} - F_{ref}$  shows the importance of taking into account high-  
 220 frequency variability of  $P_{atm}$ . Another difference  $\overline{F_{p,T}} - \overline{F_p}$  reflects the importance of taking  
 221 into account daily  $T$ , while  $\overline{F_h} - \overline{F_{p,T}}$  shows the impact of submonthly variations of  $S$ .  
 222 Finally, the corresponding global ocean sinks of anthropogenic carbon  $S_h$  and  $S_{ref}$  are obtained  
 223 by spatially integrating the air-sea CO<sub>2</sub> flux (between 60°S and 60°N), and correcting for  
 224 preindustrial outgassing by subtracting the global  $S_{river} = 0.65 \pm 0.15 PgCyr^{-1}$  (Regnier et  
 225 al., 2022).

226 We consider that the differences  $\overline{F_h} - F_{ref}$  and  $S_h - S_{ref}$  are statistically significant only  
 227 if they differ from 0 at the 99% level using Student's t-test.

## 228 2.2 Reynolds decomposition

229 To investigate the non-linearities between high-frequency variations of the variables that  
 230 are responsible for differences between  $F_{ref}$  and  $\overline{F_h}$ , a Reynolds decomposition is used with  
 231 respect to  $u$  and  $\Delta = fCO_{2atm} - fCO_{2sea}$  for each month from 2009 to 2018, assuming that  
 232 the solubility and Schmidt number variations cancel out to give  $A = \overline{A}$  (Etcheto et Merlivat  
 233 1988), an assumption good to within 5% locally (Wanninkhof, 2014):

$$234 \quad F_h = aA\overline{u}^2\overline{\Delta} + aA(u')^2\overline{\Delta} + 2aA\overline{u}u'\Delta' + aA(u')^2\Delta' + aA\overline{u}^2\Delta' + 2aA\overline{u}u' \quad (5)$$

235 whose monthly mean is

$$236 \quad \overline{F_h} = \underbrace{aA\overline{u}^2\overline{\Delta}}_{\text{bulkterm}} + \underbrace{aA\overline{(u')^2}\overline{\Delta}}_{\text{variance}} + \underbrace{2aA\overline{u}u'\Delta'}_{\text{covariance}} + \underbrace{aA\overline{(u')^2}\Delta'}_{\text{3rdordermoment}} \quad (6)$$

237 The combination of the first term (mean bulk) and 2nd term (variance) is referred to as  
 238 the bulk term ( $aA\overline{u^2\Delta} = aA\overline{u^2}\overline{\Delta} + aA\overline{(u')^2\Delta}$ ). Thus by definition it includes the enhancement  
 239 from wind speed variance. The bulk term is very close to the reference flux  $F_{ref}$ . This agreement  
 240 along with the assumption that  $A = \overline{A}$  is illustrated by the mean difference between  $F_{ref}$  and  
 241 the bulk term ( $aA\overline{u^2\Delta}$ ), which ranges from 0 to - 0.2 g C m<sup>-2</sup> yr<sup>-1</sup> (Figure S1), an order of  
 242 magnitude smaller than the mean differences between  $\overline{F_h}$  and  $F_{ref}$  (Figure 1c). This bulk term  
 243 (mean bulk and variance in (6)) is the same as the GCB flux definition. GCB and other data-  
 244 based reconstructions do not take into account the final two terms of equation (6), the correction  
 245 terms. The first of those ( $u$  and  $\Delta$  covariance term) accounts for how the flux is affected by  
 246 covariation between wind speed anomalies and  $\Delta$  anomalies (2nd-order moment). The second  
 247 of the correction terms (3rd-order mixed moment) accounts for nonlinear interactions between  
 248 wind speed variance and  $\Delta$  anomalies, thus capturing effects from skewness or asymmetry in  
 249 fluctuations.

### 250 3. Results

#### 251 3.1 Global ocean carbon sink sensitivity to submonthly variability

252 Our estimate  $S_{ref}$  is comparable in magnitude to the average from the GCB data  
 253 products although it does not capture the precise interannual evolution, in particular after 2016  
 254 (Figure 1a). This difference stems from the latest version of the DIC and Alk OceanSODA-  
 255 ETHZ dataset (v2021, Gregor et al. 2021), which does not capture the change in Alk, DIC and  
 256  $fCO_{2sea}$  associated with the slowdown in ocean sink after 2016 (e.g. Friedlingstein et al. 2022).  
 257 This slowdown indeed only emerged in GCB data-based products after GCB 2023 (e.g.  
 258 Friedlingstein et al. 2025). Both our  $S_{ref}$  and GCB account for submonthly variability of  $u$ .  
 259 Our sink estimate  $S_h$  also accounts for submonthly variability of  $P_{atm}$ ,  $T$ , and  $S$ , and it is 0.12  
 260 Pg C yr<sup>-1</sup> lower than  $S_{ref}$ . Therefore, the standard approach, which neglects all submonthly

261 variability besides that of  $u$ , overestimates the carbon sink by  $0.12 \text{ Pg C yr}^{-1}$ . On average  
262 between 2009 and 2018, this difference corresponds to 5% of the carbon sink  $S_{ref}$  but 25% of  
263 the discrepancy between models and data products from GCB ( $\sim 0.5 \text{ Pg C yr}^{-1}$ ). Our computed  
264 difference does not change over 2009 to 2018 and remains statistically significant.

265 The spatial distribution of  $F_{ref}$  (Fig. 1b) is consistent with the fluxes from the SeaFlux  
266 product (Fay et al. 2021, Figure S2). The 2009-2018 mean difference  $\overline{F_h} - F_{ref}$  shows that the  
267 discrepancy between the two fluxes stems largely from latitudes between  $30^\circ$  and  $60^\circ$  in both  
268 hemispheres (Figure 1c). In these regions relative to  $F_{ref}$ ,  $\overline{F_h}$  exhibits either more outgassing  
269 (North Atlantic, Southern Ocean) or less uptake (North Pacific, by  $1.5 \text{ g C m}^{-2} \text{ yr}^{-1}$  on average).  
270 A weaker opposing effect is seen in tropics, where sinks are increased by  $0.5 \text{ g C m}^{-2} \text{ yr}^{-1}$  on  
271 average, and by up to  $1 \text{ g C m}^{-2} \text{ yr}^{-1}$  in the Arabian Sea and South China Sea.

272 Differences in the mid-latitudes are mainly due to atmospheric pressure variations,  
273 whereas differences in the tropics are driven by sea surface temperature variations. The former  
274 can be seen in the  $\overline{F_p} - F_{ref}$  map (Figure 2a) and the  $\overline{F_{p,T}} - \overline{F_p}$  map (Figure 2b). Atmospheric  
275 pressure variations reduce the carbon sink estimate by  $0.136 \text{ Pg C yr}^{-1}$  on average, an effect that  
276 is slightly weakened by sea surface temperature variations which increase the sink by  $0.016 \text{ Pg}$   
277  $\text{C yr}^{-1}$ . On synoptic timescales (2-10 days), low pressure perturbations are associated with  
278 stronger winds, so periods of strong  $\text{CO}_2$  exchange have lower atmospheric pressure and thus  
279 lower atmospheric  $\text{CO}_2$  fugacity. Thus wind speed and atmospheric pressure covariance leads  
280 to an anomalous outgassing correction term in the midlatitudes. Further separation of  $\overline{F_{p,T}} -$   
281  $\overline{F_p}$  into atmospheric and oceanic components (Figure S3b) reveal that temperature variations  
282 mainly affect ocean  $f\text{CO}_{2,sea}$ , but have negligible effect on vapor pressure. The anomalous  
283 ingassing in the Arabian Sea appears to result from an increase in submonthly variability of

284 wind speed, which drives stronger upwelling and hence surface cooling, thus reducing  $fCO_{2sea}$ .  
285 The remaining effect of salinity ( $\overline{F_h} - \overline{F_{P,T}}$ ) is negligible.

286

### 287 **3.2 Relative importance of the correction terms**

288 The Reynolds decomposition (5) reveals the relative importance of the different terms  
289 in equation (5). The wind speed variance term, which is already accounted for in the GCB data-  
290 based products, is the dominant source of submonthly nonlinearity (Fig 3a). It results in an  
291 increase in the estimated 60°N-60°S ocean carbon sink by 0.36 Pg C yr<sup>-1</sup>. This increase is  
292 situated mainly in the mid-latitudes, peaking at 40°S and 40°N (Fig. 3, S4).

293 Our first correction term (covariance) accounts for 90% of the correction, whereas the  
294 third-order moment is weaker. Together they result in a global outgassing anomaly whose  
295 magnitude is one-third of the wind variance term and opposite in sign. About 85% of this  
296 contribution is situated between 60°-30°S and amounts to a reduction of 0.1 Pg C yr<sup>-1</sup> (Fig. 3a).  
297 The other main region where the correction terms reduce the sink is between 30°-60°N, but that  
298 reduction of 0.03 Pg C yr<sup>-1</sup> is largely offset by the 0.026 Pg C yr<sup>-1</sup> increase between 30°S-30°N.  
299 Although the covariance term is generally weaker than the wind speed variance term, it has a  
300 similar magnitude in the tropics and dominates south of 50°S (Figure 3b).

## 301 **4. Discussion**

302 This study reveals that accounting for hourly variability in atmospheric pressure and  
303 including the small compensation from daily variability in sea surface temperature, reduces  
304 data-based estimates of the global ocean carbon sink by 0.12 Pg C yr<sup>-1</sup>, thereby closing 25%  
305 of the gap between those data products and the GOBMs. While the 8-day product from Gregor  
306 et al. (2024) offers higher frequency atmospheric and oceanic CO<sub>2</sub> fugacities than the standard

307 monthly products used in the GCB data-based ocean flux estimates, the resulting computed  
308 global flux is essentially unchanged. Thus, it appears that at least synoptic frequency is needed  
309 to adequately capture the effect of atmospheric variability. Whether or not 6-hourly or daily  
310 atmospheric pressure data would be sufficient in place of our use of hourly data remains a  
311 question for future research.

312 The Reynolds decomposition of the high-resolution CO<sub>2</sub> flux confirms that the submonthly  
313 variation in wind speed, already accounted for in the ocean data products, is the most important  
314 nonlinearity. It generally increases sink estimates outside the tropics with peaks at 40°S and  
315 40°N. Conversely, our correction due to the submonthly covariance of wind speed and  
316 atmospheric pressure leads to outgassing anomalies in the midlatitudes. The reason is that  
317 midlatitude synoptic disturbances have strong winds that favor air-sea exchange but also reduce  
318 atmospheric pressure, thus lowering atmospheric CO<sub>2</sub> fugacity, which favors outgassing. This  
319 correction is particularly large in waters south of 30°S, representing 85% of its impact on the  
320 global ocean carbon sink. South of 50°S, it becomes the main source of nonlinearity.

321 While the nonlinearities underlined here appear to explain 25% of the average gap between  
322 models and data-based products, their effect seems constant in time. Therefore, they do not  
323 seem to explain the temporal evolution of the gap underlined by Friedlingstein et al. (2025).  
324 The exact correction will depend on the calculation details and thus will differ between data-  
325 based products. For future GCB exercises, we suggest that each group compute independently  
326 both directions of the flux  $k_{660}(u)A(T, S)fCO_{2atm}$  and  $k_{660}(u)A(T, S)fCO_{2sea}$  at maximum  
327 temporal resolution before computing monthly averages and taking the difference to obtain the  
328 flux. We also leave for future studies the question of whether or not accounting for submonthly  
329 variations in atmospheric  $X_{CO_2}$ , particularly those due to covariations with  $P_{atm}$ , may  
330 substantially alter data-based estimates of ocean carbon uptake. The gap between data-based  
331 products and GOBMs also depends on model resolution and their representation of coastal

332 regions (e.g. Resplandy et al. 2024) as well as on processes not yet commonly included in the  
333 flux parameterization, such as the ocean cool skin (+0.3 Pg C yr<sup>-1</sup>, Dong et al. 2022), rain  
334 (+0.14-0.19 Pg C yr<sup>-1</sup>, Parc et al. 2024) and wave breaking-induced bubbles. While these  
335 bubbles may increase modeled CO<sub>2</sub> uptake by only 0.07 Pg C yr<sup>-1</sup> (Rustogi et al., 2025), they  
336 could increase data-based estimates by up to 0.3-0.4 Pg C yr<sup>-1</sup> (Dong et al., 2025). Similarly,  
337 Bellenger et al. (2023) showed that the cool skin temperature effect is three times smaller in a  
338 model framework because of the feedback process mentioned earlier and because gas exchange  
339 is not rate limiting, unlike carbon transfer to the ocean interior. Including the cool skin effect in  
340 both data-based products and GOBMs could thus increase the gap by about +0.2 Pg C yr<sup>-1</sup>. The  
341 addition of new processes in the calculation of carbon fluxes may further increase the gap  
342 between estimates from data-based products versus GOBMs.

343 Our results suggest that the previous estimate of the storm-induced outgassing for the Southern  
344 Ocean of 0.057 Pg C yr<sup>-1</sup> (Carranza et al., 2024) is only a fraction of the total effect of  
345 submonthly variability on the ocean sink in this region. Indeed, we found a mean outgassing of  
346 about 0.1 Pg C yr<sup>-1</sup> in the 60°-30°S band mainly driven by atmospheric pressure and wind speed  
347 covariance. On the other hand, previous observations in the Southern Ocean from Argo floats  
348 (Carranza et al., 2024) and gliders (Nicholson et al., 2022) suggest that submonthly variability  
349 of ocean biogeochemical variables have a major impact on storm induced outgassing. Those  
350 observations suggest that entrainment of cold, DIC-rich subsurface water into the surface mixed  
351 layer is the leading cause of mean storm-driven CO<sub>2</sub> outgassing in the Southern Ocean  
352 (Carranza et al., 2024). Monthly  $fCO_2$ -products cannot resolve storm induced  $fCO_{2sea}$ , while  
353 GOBMs may underestimate storm-driven vertical transport of DIC (Carranza et al. 2024).  
354 Therefore, submonthly variability of biogeochemical variables in the Southern Ocean demands  
355 more attention, both for data- and model-based estimates. While our study helps to narrow the  
356 data-model gap, its continued growth and the large disparities among data-based products and

357 among models underscore the need for further advances to constrain ocean carbon uptake,  
358 advances that are also key to reducing, by difference, much larger uncertainties associated with  
359 the terrestrial biosphere.

360 **Author contributions:** Conceptualization JD, HB, XP, JCO; Methodology: LP, XP, JCO,  
361 Formal analysis: JD, XP, HB; Visualization: JD; Writing: JD, HB, JCO, LK, FC, LB, MG, RS,  
362 SB.

### 363 **Acknowledgments**

364 This study has been conducted using EU Copernicus Marine Service Information;  
365 <https://doi.org/10.48670/moi-00051>. To process the data, this study benefited from the IPSL  
366 mesocenter ESPRI facility which is supported by CNRS, UPMC, Labex L-IPSL, CNES and  
367 Ecole Polytechnique. JCO and MG were funded by EU grant 101083922 (OceanICU). RS  
368 acknowledges funding from the EU's Horizon Europe research and innovation programme  
369 under ESM2025 (grant agreement No 101003536) and OptimESM (grant agreement No  
370 101081193) as well as the ANR - France 2030 as part of the PEPR TRACCS programme under  
371 grant number ANR-22-EXTR-0009.

### 372 **Data availability**

373 Estimates of the CO<sub>2</sub> fluxes for the different diagnostics made here are publicly available at  
374 the Zenodo repository <https://doi.org/10.5281/zenodo.15848192>. ERA5 reanalysis data from  
375 the ECMWF (Hersbach, H. et al., 2020) was obtained through the Copernicus Climate  
376 Change Service (C3S, 2023) ([https://cds.climate.copernicus.eu/cdsapp#!/dataset/reanalysis-  
377 era5-single-levels](https://cds.climate.copernicus.eu/cdsapp#!/dataset/reanalysis-era5-single-levels)). The results contain modified Copernicus Climate Change Service  
378 information 2020. Neither the European Commission nor ECMWF is responsible for any use  
379 that may be made of the Copernicus information or data it contains. The CO<sub>2</sub> dry air mole  
380 fraction data are from the NOAA Greenhouse Gas Marine Boundary Layer Reference

381 (<https://gml.noaa.gov/ccgg/mbl/data.php>). The sea surface salinity values were downloaded  
382 from EU Copernicus Marine Service Information (<https://doi.org/10.48670/moi-00051>).  
383 Global DIC and Alk bulk values are from the OceanSODA–ETHZ climatology dataset  
384 ([https://www.ncei.noaa.gov/access/metadata/landing-  
386 page/bin/iso?id=gov.noaa.nodc:0220059](https://www.ncei.noaa.gov/access/metadata/landing-<br/>385 page/bin/iso?id=gov.noaa.nodc:0220059)). The Broullón et al. (2020) monthly climatologies  
387 of dissolved inorganic silicon and phosphorus are available at  
<https://digital.csic.es/handle/10261/184460>.

388

## 389 **References**

- 390 Aumont, O., Orr, J. C., Monfray, P., Ludwig, W., Amiotte-Suchet, P., and Probst, J.-L., 2001:  
391 Riverine-driven interhemispheric transport of carbon, *Global Biogeochem. Cy.*, 15,  
392 393–405, <https://doi.org/10.1029/1999GB001238>
- 393 Bakker, D. C. E., Pfeil, B., Landa, C. S., Metzl, N., O’Brien, K. M., Olsen, A., Smith, K., Cosca,  
394 C., Harasawa, S., Jones, S. D., Nakaoka, S., Nojiri, Y., Schuster, U., Steinhoff, T.,  
395 Sweeney, C., Takahashi, T., Tilbrook, B., Wada, C., Wanninkhof, R., ... Xu, S. (2016).  
396 A multi-decade record of high-quality fCO<sub>2</sub> data in version 3 of the Surface Ocean CO<sub>2</sub>  
397 Atlas (SOCAT). *Earth System Science Data*, 8(2), 383–413.  
398 <https://doi.org/10.5194/essd-8-383-2016>
- 399 Bates, N. R., Knap, A. H., & Michaels, A. F. (1998). Contribution of hurricanes to local and  
400 global estimates of air–sea exchange of CO<sub>2</sub>. *Nature*, 395(6697), 58–61.  
401 <https://doi.org/10.1038/25703>
- 402 Bellenger, H., Bopp, L., Ethé, C., Ho, D., Duvel, J. P., Flavoni, S., Guez L., T. Kataoka, X.  
403 Perrot, L. Parc, and M. Watanabe (2023). Sensitivity of the global ocean carbon sink to  
404 the ocean skin in a climate model. *Journal of Geophysical Research : Oceans*, 128,  
405 e2022JC019479. <https://doi.org/10.1029/2022JC019479>

406 Boyer, T.P., Antonov, J.I., Baranova, O.K., Coleman, C., Garcia, H.E., Grodsky, A., Johnson,  
407 D.R. Locarnini, R.A., Mishonov, A.V., O'Brien, T.D., Paver, C.R., Reagan, J.R., Seidov,  
408 D., Smolyar, I.V. and Zweng, M.M. (2013) World Ocean Database 2013. Silver Spring,  
409 MD, National Oceanographic Data Center, 208pp. (NOAA Atlas NESDIS, 72). DOI:  
410 <https://doi.org/10.25607/OBP-1454>

411 Bronselaer, B., Winton, M., Russell, J., Sabine, C. L., & Khatiwala, S. (2017). Agreement of  
412 CMIP5 simulated and observed ocean anthropogenic CO<sub>2</sub> uptake. *Geophysical*  
413 *Research Letters*, 44, 12,298–12,305. <https://doi.org/10.1002/2017GL074435>

414 Broullón, D., Pérez, F. F., Velo, A., Hoppema, M., Olsen, A., Takahashi, T., Key, R. M.,  
415 Tanhua, T., González-Dávila, M., Jeansson, E., Kozyr, A., & van Heuven, S. M. A. C.  
416 (2019). A global monthly climatology of total alkalinity: A neural network approach.  
417 *Earth System Science Data*, 11(3), 1109–1127. [https://doi.org/10.5194/essd-11-1109-](https://doi.org/10.5194/essd-11-1109-2019)  
418 [2019](https://doi.org/10.5194/essd-11-1109-2019)

419 Carranza, M. M., Long, M. C., Di Luca, A., Fassbender, A. J., Johnson, K. S., Takeshita, Y.,  
420 Mongwe, P., & Turner, K. E. (2024). Extratropical storms induce carbon outgassing  
421 over the Southern Ocean. *Npj Climate and Atmospheric Science*, 7(1), 1–16.  
422 <https://doi.org/10.1038/s41612-024-00657-7>

423 Chau, T.-T.-T., Chevallier, F., & Gehlen, M. (2024). Global analysis of surface ocean CO<sub>2</sub>  
424 fugacity and air-sea fluxes with low latency. *Geophysical Research Letters*, 51,  
425 e2023GL106670. <https://doi.org/10.1029/2023GL106670>

426 DeVries, T., Yamamoto, K., Wanninkhof, R., Gruber, N., Hauck, J., Müller, J. D., et al. (2023).  
427 Magnitude, trends, and variability of the global ocean carbon sink from 1985 to 2018.  
428 *Global Biogeochemical Cycles*, 37, e2023GB007780.  
429 <https://doi.org/10.1029/2023GB007780>

430 Dong, Y., Bakker, D. C. E., Bell, T. G., Huang, B., Landschützer, P., Liss, P. S., & Yang, M.  
431 (2022). Update on the temperature corrections of global air-sea CO<sub>2</sub> flux estimates.  
432 *Global Biogeochemical Cycles*, 36, e2022GB007360.  
433 <https://doi.org/10.1029/2022GB007360>

434 Dong, Y., Yang, M., Bell, T. G., Marandino, C. A., & Woolf, D. K. (2025). Asymmetric bubble-  
435 mediated gas transfer enhances global ocean CO<sub>2</sub> uptake. *Nature Communications*,  
436 16(1), 10595. <https://doi.org/10.1038/s41467-025-66652-5>

437 Droghei, R., Buongiorno Nardelli, B., & Santoleri, R. (2018). A New Global Sea Surface  
438 Salinity and Density Dataset From Multivariate Observations (1993–2016). *Frontiers*  
439 *in Marine Science*, 5. <https://doi.org/10.3389/fmars.2018.00084>

440 Etcheto, J., et L. Merlivat. 1988. « Satellite Determination of the Carbon Dioxide Exchange  
441 Coefficient at the Ocean-Atmosphere Interface: A First Step ». *Journal of Geophysical*  
442 *Research: Oceans* 93 (C12): 15669-78. <https://doi.org/10.1029/JC093iC12p15669>.

443 Fay, A. R., Gregor, L., Landschützer, P., McKinley, G. A., Gruber, N., Gehlen, M., Iida, Y.,  
444 Laruelle, G. G., Rödenbeck, C., Roobaert, A., & Zeng, J. (2021). SeaFlux:  
445 Harmonization of air–sea CO<sub>2</sub> fluxes from surface pCO<sub>2</sub> data products using a  
446 standardized approach. *Earth System Science Data*, 13(10), 4693–4710.  
447 <https://doi.org/10.5194/essd-13-4693-2021>

448 Ford, D. J., J. Blannin, J. Watts, A. J. Watson, P. Landschützer, A. Jersild, and J. D. Shutler,  
449 2024: A comprehensive analysis of air-sea CO<sub>2</sub> flux uncertainties constructed from  
450 surface ocean data products, *Glob. Biogeochem. Cycles*, 38, e2024GB008188.  
451 <https://doi.org/10.1029/2024GB008188>

452 Friedlingstein, P., Jones, M. W., O'Sullivan, M., Andrew, R. M., Bakker, D. C. E., Hauck, J.,  
453 Le Quéré, C., Peters, G. P., Peters, W., Pongratz, J., Sitch, S., Canadell, J. G., Ciais, P.,

454 Jackson, R. B., Alin, S. R., .... Zeng, J.(2022): Global Carbon Budget 2021, *Earth Syst.*  
455 *Sci. Data*, 14, 1917–2005, <https://doi.org/10.5194/essd-14-1917-2022>.

456 Friedlingstein, P., O’Sullivan, M., Jones, M. W., Andrew, R. M., Hauck, J., Landschützer, P.,  
457 Le Quéré, C., Li, H., Lujikx, I. T., Olsen, A., Peters, G. P., Peters, W., Pongratz, J.,  
458 Schwingshackl, C., Sitch, S., Canadell, J. G., Ciais, P., Jackson, R. B., Alin, S. R., ...  
459 Zeng, J. (2025a). Global Carbon Budget 2024. *Earth System Science Data*, 17(3), 965–  
460 1039. <https://doi.org/10.5194/essd-17-965-2025>

461 Gloege, L., Yan, M., Zheng, T., & McKinley, G. A. (2022). Improved Quantification of Ocean  
462 Carbon Uptake by Using Machine Learning to Merge Global Models and pCO<sub>2</sub> Data.  
463 *Journal of Advances in Modeling Earth Systems*, 14(2), e2021MS002620.  
464 <https://doi.org/10.1029/2021MS002620>

465 Gloege, L., and Eisaman, M. D. (2025). Regional uncertainty analysis in the air–sea CO<sub>2</sub> flux.  
466 *Earth and Space Science*, 12, e2024EA004032. <https://doi.org/10.1029/2024EA004032>

467 Gregor, L., Lebehot, A. D., Kok, S., & Scheel Monteiro, P. M. (2019). A comparative  
468 assessment of the uncertainties of global surface ocean CO<sub>2</sub> estimates using a machine-  
469 learning ensemble (CSIR-ML6 version 2019a) – have we hit the wall? *Geoscientific*  
470 *Model Development*, 12(12), 5113–5136. <https://doi.org/10.5194/gmd-12-5113-2019>

471 Gregor, L., & Gruber, N. (2021). OceanSODA-ETHZ: A global gridded data set of the surface  
472 ocean carbonate system for seasonal to decadal studies of ocean acidification. *Earth*  
473 *System Science Data*, 13(2), 777–808. <https://doi.org/10.5194/essd-13-777-2021>

474 Gregor, L., Shutler, J., & Gruber, N. (2024). High-Resolution Variability of the Ocean Carbon  
475 Sink. *Global Biogeochemical Cycles*, 38(8), e2024GB008127.  
476 <https://doi.org/10.1029/2024GB008127>

477 Hauck, J., Zeising, M., Le Quéré, C., Gruber, N., Bakker, D. C. E., Bopp, L., Chau, T. T. T.,  
478 Gürses, Ö., Ilyina, T., Landschützer, P., Lenton, A., Resplandy, L., Rödenbeck, C.,

479 Schwinger, J., & Séférian, R. (2020). Consistency and Challenges in the Ocean Carbon  
480 Sink Estimate for the Global Carbon Budget. *Frontiers in Marine Science*, 7.  
481 <https://doi.org/10.3389/fmars.2020.571720>

482 Hauck, J., Nissen, C., Landschützer, P., Rödenbeck, C., Bushinsky, S., & Olsen, A. (2023).  
483 Sparse observations induce large biases in estimates of the global ocean CO<sub>2</sub> sink: an  
484 ocean model subsampling experiment. *Philosophical Transactions of the Royal Society*  
485 *A: Mathematical, Physical and Engineering Sciences*,  
486 381(2249). <https://doi.org/10.1098/rsta.2022.0063>

487 Hersbach, H., Bell, B., Berrisford, P., Hirahara, S., Horányi, A., Muñoz-Sabater, J., Nicolas, J.,  
488 Peubey, C., Radu, R., Schepers, D., Simmons, A., Soci, C., Abdalla, S., Abellan, X.,  
489 Balsamo, G., Bechtold, P., Biavati, G., Bidlot, J., Bonavita, M., ... Thépaut, J.-N.  
490 (2020). The ERA5 global reanalysis. *Quarterly Journal of the Royal Meteorological*  
491 *Society*, 146(730), 1999–2049. <https://doi.org/10.1002/qj.3803>

492 Huang, P., & Imberger, J. (2010). Variation of pCO<sub>2</sub> in ocean surface water in response to the  
493 passage of a hurricane. *Journal of Geophysical Research - Oceans*, 115(C10024),  
494 Article number C10024, 11pp. <https://doi.org/10.1029/2010JC006185>

495 Iida, Y., Takatani, Y., Kojima, A., & Ishii, M. (2021). Global trends of ocean CO<sub>2</sub> sink and  
496 ocean acidification: An observation-based reconstruction of surface ocean inorganic  
497 carbon variables. *Journal of Oceanography*, 77, 323–358.  
498 <https://doi.org/10.1007/s10872-020-00571-5>

499 Jersild, A., and Landschützer, P. (2024). A spatially explicit uncertainty analysis of the air-sea  
500 CO<sub>2</sub> flux from observations. *Geophysical Research Letters*, 51,  
501 e2023GL106636. <https://doi.org/10.1029/2023GL106636>

502 Lan, X., Tans, P., Thoning, K., NOAA Global Monitoring, & Laboratory. (2023). MBL  
503 Reference—*NOAA Global Monitoring Laboratory* [Dataset].  
504 <https://doi.org/10.15138/DVNP-F961>

505 Landschützer, P., Gruber, N., & Bakker, D. C. E. (2016). Decadal variations and trends of the  
506 global ocean carbon sink. *Global Biogeochemical Cycles*, 30(10), 1396–1417.  
507 <https://doi.org/10.1002/2015GB005359>

508 Lévy, M., Lengaigne, M., Bopp, L., Vincent, E. M., Madec, G., Ethé, C., Kumar, D., & Sarma,  
509 V. V. S. S. (2012). Contribution of tropical cyclones to the air-sea CO<sub>2</sub> flux: A global  
510 view. *Global Biogeochemical Cycles*, 26(2). <https://doi.org/10.1029/2011GB004145>

511 Naegler, T. (2009). Reconciliation of excess<sup>14</sup>C-constrained global CO<sub>2</sub> piston velocity  
512 estimates. *Tellus B: Chemical and Physical Meteorology*, 61(2), 372.  
513 <https://doi.org/10.1111/j.1600-0889.2008.00408.x>

514 Nicholson, S.-A., Whitt, D. B., Fer, I., du Plessis, M. D., Lebéhot, A. D., Swart, S., Sutton, A.  
515 J., & Monteiro, P. M. S. (2022). Storms drive outgassing of CO<sub>2</sub> in the subpolar  
516 Southern Ocean. *Nature Communications*, 13(1), 158. [https://doi.org/10.1038/s41467-](https://doi.org/10.1038/s41467-021-27780-w)  
517 [021-27780-w](https://doi.org/10.1038/s41467-021-27780-w)

518 Orr, J. C., & Epitalon, J.-M. (2015). Improved routines to model the ocean carbonate system:  
519 mocsy 2.0. *Geoscientific Model Development*, 8(3), 485–499.  
520 <https://doi.org/10.5194/gmd-8-485-2015>

521 Parc, L., Bellenger, H., Bopp, L., Perrot, X., & Ho, D. T. (2024). Global ocean carbon uptake  
522 enhanced by rainfall. *Nature Geoscience*, 17(9), 851–857.  
523 <https://doi.org/10.1038/s41561-024-01517-y>

524 Pérez, F. F., Becker, M., Goris, N., Gehlen, M., López-Mozos, M., Tjiputra, J., et al. (2024).  
525 An assessment of CO<sub>2</sub> storage and sea-air fluxes for the Atlantic Ocean and

526 Mediterranean Sea between 1985 and 2018. *Global Biogeochemical Cycles*, 38,  
527 e2023GB007862. <https://doi.org/10.1029/2023GB007862>

528 Planchat, A., Bopp, L., & Kwiatkowski, L. (2025). A fresh look at the pre-industrial air-sea  
529 carbon flux using the alkalinity budget. *EGUsphere*, 1–50.  
530 <https://doi.org/10.5194/egusphere-2025-523>

531 Regnier, P., Resplandy, L., Najjar, R. G., & Ciais, P. (2022). The land-to-ocean loops of the  
532 global carbon cycle. *Nature*, 603(7901), 401–410. [https://doi.org/10.1038/s41586-021-](https://doi.org/10.1038/s41586-021-04339-9)  
533 04339-9

534 Resplandy, L., A. Hogikyan, J. D. Müller, R. G. Najjar, H. W. Bange, D. Bianchi, T. Weber, et  
535 al. 2024. « A Synthesis of Global Coastal Ocean Greenhouse Gas Fluxes ». *Global*  
536 *Biogeochemical Cycles* 38 (1): e2023GB007803.  
537 <https://doi.org/10.1029/2023GB007803>

538 Rödenbeck, C., DeVries, T., Hauck, J., Le Quéré, C., & Keeling, R. F. (2022). Data-based  
539 estimates of interannual sea–air CO<sub>2</sub> flux variations 1957–2020 and their relation to  
540 environmental drivers. *Biogeosciences*, 19(10), 2627–2652. [https://doi.org/10.5194/bg-](https://doi.org/10.5194/bg-19-2627-2022)  
541 19-2627-2022

542 Rustogi, P., Resplandy, L., Liao, E., Reichl, B. G., & Deike, L. (2025). Influence of wave-  
543 induced variability on ocean carbon uptake. *Global Biogeochemical Cycles*, 39,  
544 e2024GB008382. <https://doi.org/10.1029/2024GB008382>

545 Takahashi, T., Sutherland, S. C., Wanninkhof, R., Sweeney, C., Feely, R. A., Chipman, D. W.,  
546 Hales, B., Friederich, G., Chavez, F., Sabine, C., Watson, A., Bakker, D. C. E., Schuster,  
547 U., Metzl, N., Yoshikawa-Inoue, H., Ishii, M., Midorikawa, T., Nojiri, Y., Körtzinger,  
548 A., ... de Baar, H. J. W. (2009). Climatological mean and decadal change in surface  
549 ocean pCO<sub>2</sub>, and net sea–air CO<sub>2</sub> flux over the global oceans. *Deep Sea Research Part*

550 *II: Topical Studies in Oceanography, Surface Ocean CO<sub>2</sub> Variability and*  
551 *Vulnerabilities*, 56(8), 554–577. <https://doi.org/10.1016/j.dsr2.2008.12.009>

552 Terhaar, J., Frölicher, T. L., and Joos, F. 2022: Observation-constrained estimates of the global  
553 ocean carbon sink from Earth system models, *Biogeosciences*, 19, 4431–4457,  
554 <https://doi.org/10.5194/bg-19-4431-2022>.

555 Terhaar, J., Goris, N., Müller, J. D., DeVries, T., Gruber, N., Hauck, J., et al. (2024).  
556 Assessment of global ocean biogeochemistry models for ocean carbon sink estimates in  
557 RECCAP2 and recommendations for future studies. *Journal of Advances in Modeling*  
558 *Earth Systems*, 16, e2023MS003840. <https://doi.org/10.1029/2023MS003840>

559 Wanninkhof, R. (1992). Relationship between wind speed and gas exchange over the ocean.  
560 *Journal of Geophysical Research: Oceans*, 97(C5), 7373–7382.  
561 <https://doi.org/10.1029/92JC00188>

562 Wanninkhof, R. (2014). Relationship between wind speed and gas exchange over the ocean  
563 revisited. *Limnology and Oceanography: Methods*, 12(6), 351–362.  
564 <https://doi.org/10.4319/lom.2014.12.351>

565 Watson, A. J., Schuster, U., Shutler, J. D., Holding, T., Ashton, I. G. C., Landschützer, P.,  
566 Woolf, D. K., & Goddijn-Murphy, L. (2020). Revised estimates of ocean-atmosphere  
567 CO<sub>2</sub> flux are consistent with ocean carbon inventory. *Nature Communications*, 11(1),  
568 4422. <https://doi.org/10.1038/s41467-020-18203-3>

569 Weiss, R. F. (1974). Carbon dioxide in water and seawater: The solubility of a non-ideal gas.  
570 *Marine Chemistry*, 2(3), 203–215. [https://doi.org/10.1016/0304-4203\(74\)90015-2](https://doi.org/10.1016/0304-4203(74)90015-2)

571 Weiss, R. F., & Price, B. A. (1980). Nitrous oxide solubility in water and seawater. *Marine*  
572 *Chemistry*, 8(4), 347–359. [https://doi.org/10.1016/0304-4203\(80\)90024-9](https://doi.org/10.1016/0304-4203(80)90024-9)

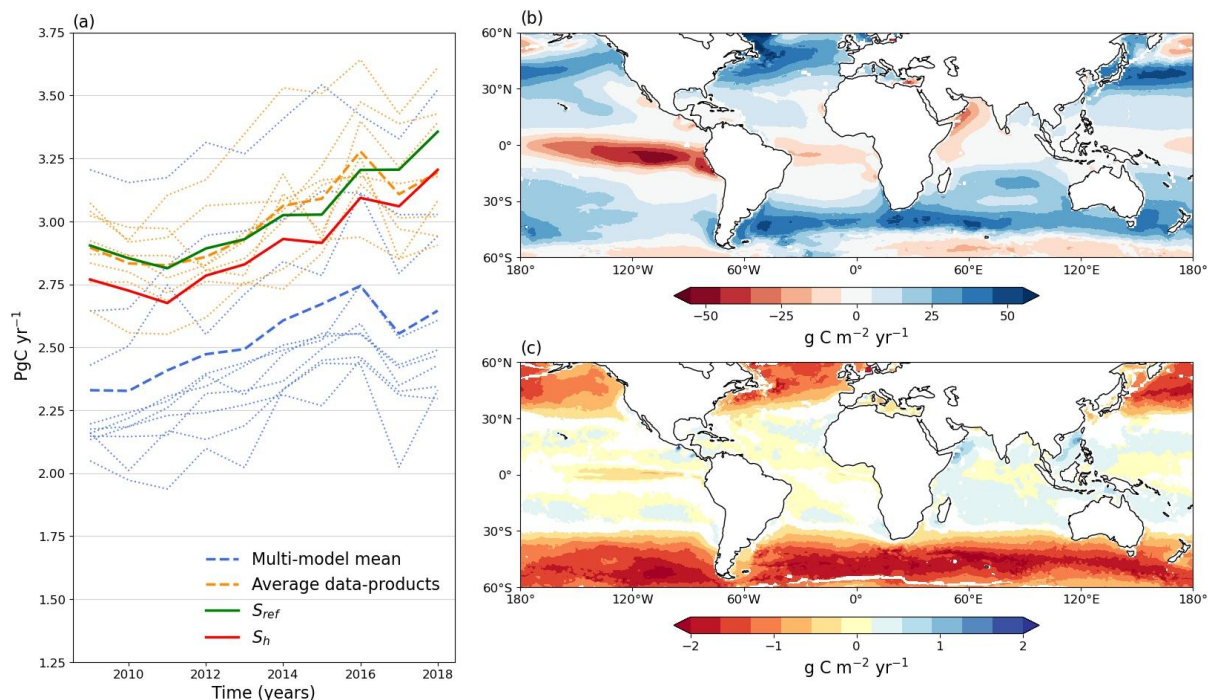
573 Wu, C., Wang, Q., Zhao, Z., & Zhang, K. (2025). Extreme CO<sub>2</sub> Release and Its Mechanism in  
574 the Subarctic North Pacific During the Winters of 1999–2001. *Journal of Geophysical*  
575 *Research: Oceans*, 130(4), e2024JC021708. <https://doi.org/10.1029/2024JC021708>  
576 Zeng, J., Iida, Y., Matsunaga, T., & Shirai, T. (2022). Surface ocean CO<sub>2</sub> concentration and  
577 air-sea flux estimate by machine learning with modelled variable trends. *Frontiers in*  
578 *Marine Science*, 9. <https://doi.org/10.3389/fmars.2022.989233>  
579  
580  
581  
582

584 **Table 1. Sources of all datasets used in this study.**

| Variable   | Description                           | Time resolution     | Source                 |
|------------|---------------------------------------|---------------------|------------------------|
| $P_{atm}$  | Surface pressure                      | Hourly              | ERA5                   |
| $u$        | 5m wind speed                         | Hourly              | ERA5                   |
| Sea ice    | Sea ice fraction                      | Hourly              | ERA5                   |
| $T$        | Sea surface temperature               | Daily               | ERA5                   |
| $S$        | Sea surface salinity                  | 8-days              | Droghei et al. (2018)  |
| DIC        | Dissolved inorganic carbon            | Monthly             | OceanSODA-ETHZ         |
| Alk        | Alkalinity                            | Monthly             | OceanSODA-ETHZ         |
| $X_{CO_2}$ | CO <sub>2</sub> dry air mole fraction | Monthly             | NOAA MBL               |
| [ $P$ ]    | Phosphate concentration               | Monthly climatology | Broullón et al. (2019) |
| [ $Si$ ]   | Silicate concentration                | Monthly climatology | Broullón et al. (2019) |

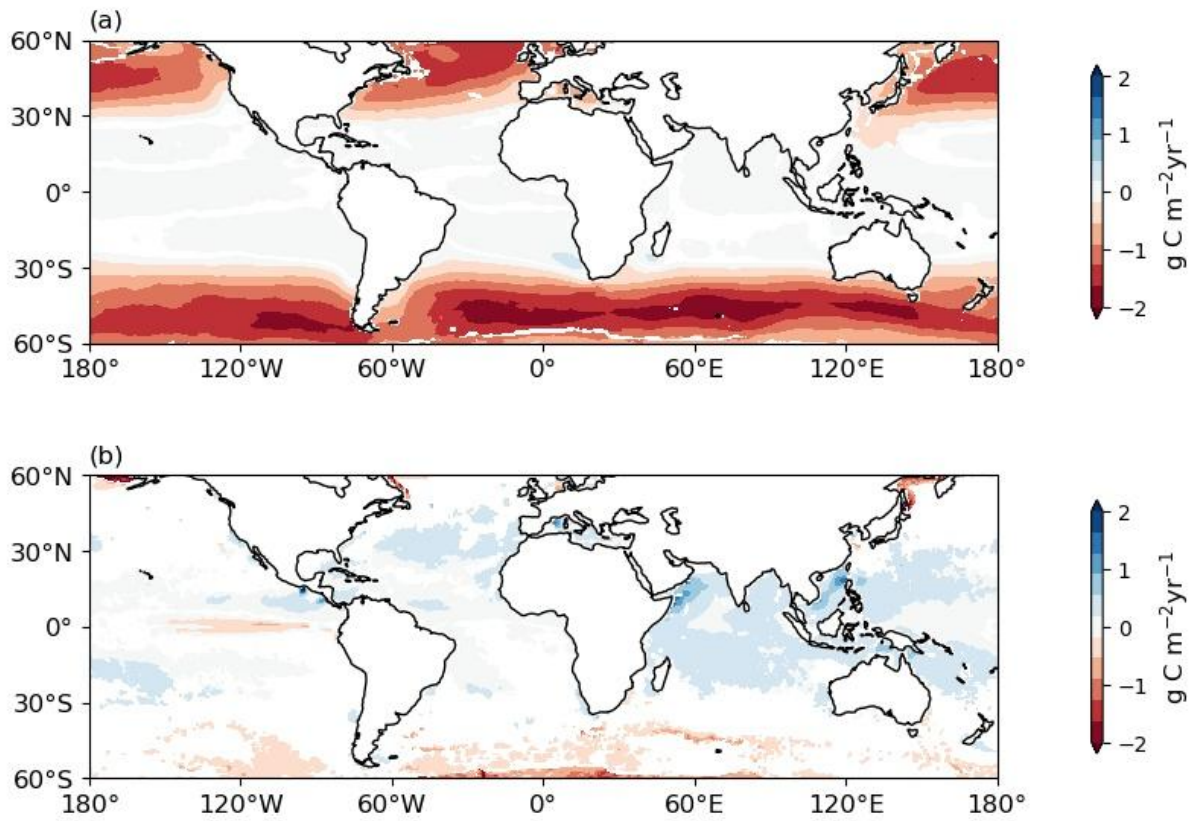
586

587 **Figures**



588

589 **Figure 1. a) Time series of the global (60°N-60°S) annual mean CO<sub>2</sub> sink (Pg C yr<sup>-1</sup>)**  
590 **computed from  $S_{ref}$  (thick green line),  $S_h$  (thick red line), and the global annual mean**  
591 **from the GCB 2024 data products (thin orange lines) and their mean (thick dashed orange**  
592 **line) as well as the GCB 2024 models (thin blue lines) and their mean (thick dashed blue**  
593 **line). Also shown are maps for the 2009-2018 mean of b) the air-sea CO<sub>2</sub> reference flux**  
594  **$F_{ref}$  and c) the difference between the monthly mean of the high frequency flux  $\overline{F_h}$  and**  
595  **$F_{ref}$ , where positive values indicate less outgassing or more uptake with  $\overline{F_h}$  than with  $F_{ref}$ .**



596

597 **Figure 2. Maps averaged over 2009-2018 for effects on observation-based air-sea CO<sub>2</sub>**

598 **fluxes from a) submonthly variability of atmospheric pressure ( $\overline{F_P} - F_{ref}$ ) and b)**

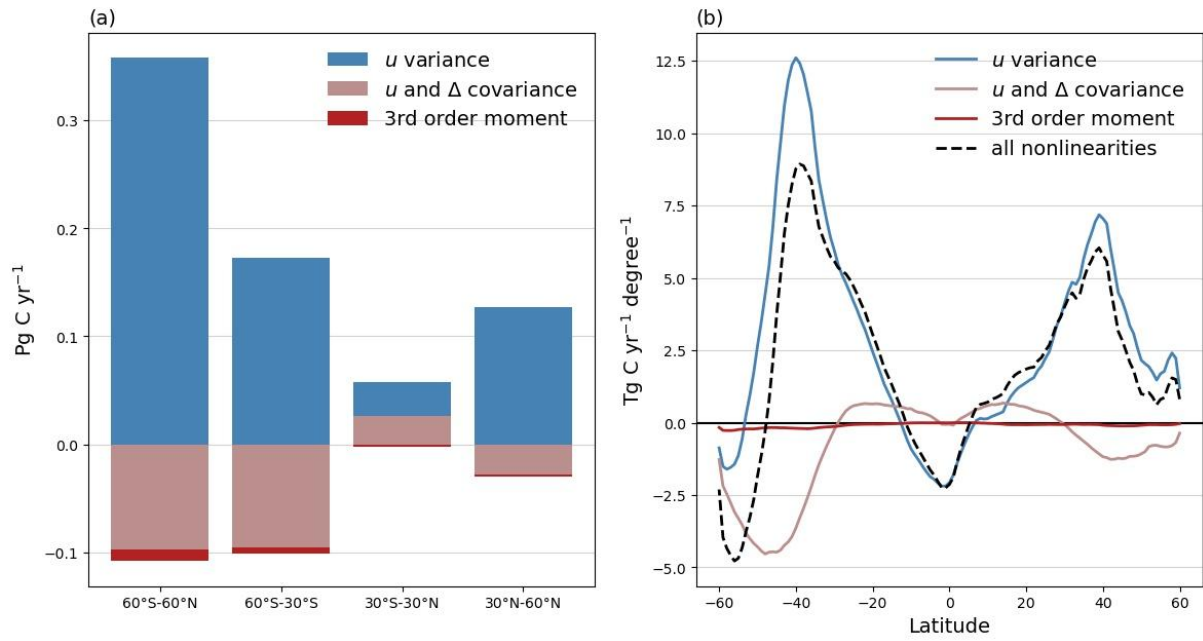
599 **submonthly variability of temperature ( $\overline{F_{P,T}} - \overline{F_P}$ ).**

600

601

602

603



604

605 **Figure 3. a) Contribution of the final 3 terms in equation 5 to ocean carbon uptake in**  
 606 **different latitudinal bands. b) Zonal integral of the final three terms in equation 5 (blue,**  
 607 **pink and red lines) and their sum (dashed black line).**